

Droplet model of the giant dipole resonance*

W. D. Myers and W. J. Swiatecki

Nuclear Science Division, Lawrence Berkeley Laboratory, University of California, Berkeley, California 94720

T. Kodama and L. J. El-Jaick

Centro Brasileiro de Pesquisas Físicas, Av. Wenceslau Braz, 71-zc-82, Rio de Janeiro, RJ 20.000, Brazil

E. R. Hilf

Institut für Kernphysik, Technische Hochschule Darmstadt, Schlossgartenstrasse 9, 6100 Darmstadt, Germany

(Received 7 December 1976)

The nuclear giant dipole resonance is discussed using a macroscopic model with two new features. The motion is treated as a combination of the usual Goldhaber-Teller displacement mode and the Steinwedel-Jensen acoustic mode, and the restoring forces are all calculated using the droplet model. The A dependence of the resonance energies is well reproduced without any adjustable parameters, and the actual magnitude of the energies serves to fix the value of the effective mass m^* used in the theory. The giant dipole resonance is found to contain a large component of the Goldhaber-Teller type of motion, with the Steinwedel-Jensen mode becoming comparable for heavy nuclei. The width Γ of the giant dipole resonance is estimated on the basis of an expression for one-body damping.

[NUCLEAR REACTIONS Semiclassical theory, nuclear giant dipole resonance,
calculated $\sigma(E)$, Γ . Droplet model restoring forces. Coupled modes.]

I. INTRODUCTION

The giant electric dipole resonance (GDR) is a beautiful example, among the vast variety of possible nuclear excitations, of a manifestly collective mode that can be understood, to a large extent, in terms of a macroscopic approach. It corresponds to the absorption of electric dipole radiation by the vibration of the neutrons against the protons and the subsequent damping of this motion into intrinsic excitation.

The GDR can be observed in every nucleus throughout the Periodic Table and very little structure is to be seen in the energy dependence of the absorption cross section, except for the lightest nuclei.¹ The absorption cross section for most nuclei follows a Lorentz curve whose mean energy E_m (see Fig. 2) varies smoothly with mass number in a manner that shows little or no dependence on nuclear shell effects.²

On the basis of a few early experiments Goldhaber and Teller³ (GT) discussed three possible macroscopic explanations for the A dependence of the resonance energy. The first postulated an elastic binding of the neutrons to the protons that would result in a resonance energy independent of A . The second proposal, later elaborated by Steinwedel and Jensen⁴ (the SJ mode), was that the resonance might consist of density vibrations of the neutron and proton fluids against each other with the surfaces fixed. This kind of motion, which

corresponds to the lowest acoustic mode in a spherical cavity, would result in a resonance energy proportional to $A^{-1/3}$. Their third suggestion, one that they chose to discuss in some detail (the GT mode), was that the neutrons and protons might behave like two separate rigid but interpenetrating density distributions. The resulting resonance, consisting of the harmonic displacement of these distributions with respect to each other, would be expected to have an energy dependence proportional to $A^{-1/6}$.

Because of the crude nature of the model and the severity of the assumptions needed to justify it, the GT mode has received relatively little attention over the years. On the other hand, the SJ mode, which also imposes a harsh and unrealistic constraint on the motion (that the vibration takes place in a rigid fixed spherical cavity), has served as the basis for a vast literature dealing with the GDR. The SJ mode has been widely applied and has been extended to deformed nuclei,⁵ to include compressibility,⁶ to include the coupling to surface vibrations,^{7,8} and other surface effects.^{9,10}

Our interest in the GDR was revived when we realized that the development of the droplet model¹¹⁻¹³ (which explicitly identifies the energy associated with displacing the surface of the neutron distribution from that of the proton distribution) would permit a more realistic calculation of the restoring force for the GT mode than the *ad hoc* procedure that was used in the original

work. We also came to realize that a much more satisfactory macroscopic description of the resonance results if it is considered to be a superposition of GT and SJ modes (see, also, Ref. 14). A moment's reflection should serve to convince the reader that in an SJ type density vibration the inertia associated with the flow of neutrons and protons would tend to carry them beyond the location of the original surface when they pile up first on one side of the nucleus and then the other. This tendency of the neutron and proton boundaries to undergo a harmonic displacement from each other is just the GT mode. The participation of this mode cannot be avoided except by the unrealistic assumption of an infinitely stiff restoring force resisting such displacements.

The work that is to be described here contains these two new features. First, all the restoring forces are calculated in terms of the droplet model. Second, the motion is considered to be a superposition of GT and SJ modes with the relative magnitudes of the two modes determined by the coupling between them and the associated forces and inertias. We find that the GDR is mainly a GT mode, but with an essential admixture of the SJ mode which increases for heavier nuclei. We also find an A dependence for the resonance energy that is intermediate between that of the GT and SJ modes, in excellent agreement with the measured trends.

II. DEGREES OF FREEDOM

To describe the motion we choose a spherical (polar) coordinate system with the z axis, which is a symmetry axis, aligned along the direction of the electric field. The equation of motion will be solved subject to the constraint that the solution can be represented by a vector

$$\underline{\alpha} = \begin{pmatrix} \alpha_1 \\ \alpha_2 \end{pmatrix} \quad (2.1)$$

times a harmonic time dependence, where the vector components α_1 and α_2 represent the amounts of the GT and SJ modes.

A. GT mode

The GT mode,³ illustrated on the left side of Fig. 1, consists of a rigid displacement of the neutrons from the protons by an amount

$$d = \alpha_1 R, \quad (2.2)$$

where R is the mean radius of the nucleus. The protons and neutrons are displaced from the origin by the amounts

$$d_z = \frac{N}{A} d \quad \text{and} \quad d_n = -\frac{Z}{A} d, \quad (2.3)$$

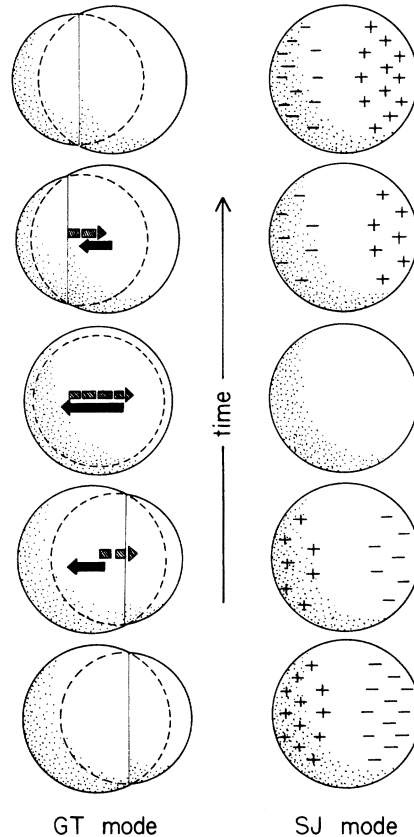


FIG. 1. Schematic drawings that serve to illustrate the general features of the Goldhaber-Teller (Ref. 3) (GT) and Steinwedel-Jensen (Ref. 4) (SJ) dipole modes. For each case, one-half cycle of the vibration is shown as a function of time. In the GT mode a uniform proton distribution (the smaller sphere whose motion is indicated by the solid arrow) vibrates against the neutron distribution. In the SJ mode the neutrons tend to pile up first on one side of the nucleus and then the other (density excess is indicated by plus signs and density reduction by minus signs). The protons (not shown) move in the opposite direction so the total density remains uniform.

which leaves the center of mass fixed.

The dipole moment is given by

$$D_1 = Ze d_z = \alpha_1 \frac{NZ}{A} eR, \quad (2.4)$$

where e is the unit of electronic charge.

The flow fields for the protons and neutrons in the GT mode are given by the velocity vectors $\vec{v}_{1n}(r, \theta)$ and $\vec{v}_{1z}(r, \theta)$, where

$$\vec{v}_{1z} = \frac{N}{A} \vec{v}_1 \quad \text{and} \quad \vec{v}_{1n} = -\frac{Z}{A} \vec{v}_1, \quad (2.5)$$

with

$$\vec{v}_1 = \dot{\alpha}_1 R (\cos\theta \hat{e}_r - \sin\theta \hat{e}_\theta), \quad (2.6)$$

where \hat{e}_r , \hat{e}_θ are unit vectors in the r and θ directions.

B. SJ mode

In the SJ mode,⁴ illustrated on the right side of Fig. 1, the protons and neutrons vibrate against each other in a fixed spherical cavity in such a way that their density variations are given by

$$\delta\rho_p = \frac{N}{A} \rho_p \delta\eta \quad \text{and} \quad \delta\rho_n = -\frac{Z}{A} \rho_n \delta\eta, \quad (2.7)$$

where

$$\delta\eta = \alpha_2 K j_1(kr) \cos\theta, \quad (2.8)$$

where

$$kR = a = 2.081576 \quad (2.9)$$

and

$$K = 2a/j_0(a) = 9.93. \quad (2.10)$$

The expressions j_0 and j_1 are spherical Bessel functions. Equation (2.9) follows from the boundary condition of zero normal velocity across the spherical boundary, which requires that the derivative of j_1 at kR , i.e., $j_1'(a)$, be zero. The normalizing coefficient K in Eq. (2.8) for the amplitude $\delta\eta$ has been chosen so that the expression for the dipole moment in the SJ mode is

$$D_2 = \alpha_2 \frac{NZ}{A} eR, \quad (2.11)$$

in analogy with Eq. (2.4). This normalization is important since it establishes a scale against which the relative contributions of GT and SJ modes to the GDR can be measured. With our choice of normalization a GT mode specified by α_1 and an SJ mode specified by α_2 have the same dipole moments if $\alpha_1 = \alpha_2$.

The velocity fields for the protons and neutrons in the SJ mode are given by

$$\vec{v}_{2p} = \frac{N}{A} \vec{v}_2 \quad \text{and} \quad \vec{v}_{2n} = -\frac{Z}{A} \vec{v}_2, \quad (2.12)$$

where

$$\vec{v}_2 = \dot{\alpha}_2 \frac{K}{k} \left[j_1'(kr) \cos\theta \hat{e}_r - \frac{1}{kr} j_1(kr) \sin\theta \hat{e}_\theta \right]. \quad (2.13)$$

III. EQUATION OF MOTION

The homogeneous equation of motion for harmonic vibrations of the system is

$$(\omega^2 \underline{B} - \underline{C}) \cdot \underline{\alpha} = 0, \quad (3.1)$$

where B and C are the inertia and stiffness matrices defined in terms of the kinetic energy T and

the potential energy V by the expressions,

$$T = \frac{1}{2} \underline{\dot{\alpha}} \cdot \underline{B} \cdot \underline{\dot{\alpha}} \quad \text{and} \quad V = \frac{1}{2} \underline{\alpha} \cdot \underline{C} \cdot \underline{\alpha} \quad (3.2)$$

A. Inertia matrix \underline{B}

The total kinetic energy of the system can be written

$$T = \frac{1}{2} m \int_{\text{vol}} \rho_p (\vec{v}_{1p} + \vec{v}_{2p})^2 + \rho_n (\vec{v}_{1n} + \vec{v}_{2n})^2, \quad (3.3)$$

where the ρ 's are particle number densities and m is the nucleon mass. If one substitutes from Eqs. (2.5) and (2.12), performs the indicated integrals, and then compares the resulting expression with Eq. (3.2), the components of \underline{B} are found to be

$$\begin{aligned} B_{11} &= B_0, \\ B_{12} &= B_{21} = B_0, \\ B_{22} &= \frac{1}{2} (a^2 - 2) B_0, \end{aligned} \quad (3.4)$$

where, if the quantity NZ/A^2 is set equal to $\frac{1}{4}$, we find that

$$\begin{aligned} B_0 &= \frac{1}{4} mAR^2 \\ &\approx \frac{1}{4} m r_0^2 A^{5/3}. \end{aligned} \quad (3.5)$$

In the last expression we assume that $R = R_0 \equiv r_0 A^{1/3}$, where r_0 is the nuclear radius constant of standard nuclear matter, for which we shall use the value 1.18 fm.¹³

Note that the quantity

$$\frac{1}{2} (a^2 - 2) = 1.166 \quad (3.6)$$

is fairly close to unity.

B. Stiffness matrix \underline{C}

In analogy with the determination of \underline{B} in the previous section, the values of the components of the stiffness matrix C can be determined by calculating the droplet model potential energy as a function of α_1 and α_2 and matching the coefficients of the quadratic terms to the corresponding terms in Eq. (3.2).

The droplet model expression for the dependence of the potential energy on $\underline{\alpha}$ is contained in the following equation¹²:

$$\begin{aligned} V &= \text{const} + \frac{1}{3} \pi r_0^3 \int_{\text{vol}} J \delta^2 \\ &+ \frac{1}{4\pi r_0^2} \int_{\text{surf}} (H\tau^2 + 2P\tau\delta_s^2 - G\delta_s^2). \end{aligned} \quad (3.7)$$

The quantity τ is the distance from the equivalent sharp surface of the proton distribution to that of the neutron distribution (i.e., the neutron skin

thickness t) in units of r_0 . The nuclear asymmetry δ (the relative local neutron excess) is defined by

$$\delta = (\rho_n - \rho_p) / (\rho_n + \rho_p) \quad (3.8)$$

and δ_s is the value of δ at the surface. The coefficient J is the nuclear symmetry energy coefficient and H, P, G are droplet model coefficients serving to describe the response of the surface energy to variations of τ and δ .¹¹⁻¹³

As we shall see, the special structure of the static droplet model scheme leaves its imprint also on the theory of the dynamics of the giant dipole oscillation, and it is necessary to review briefly the relevant features of the droplet model before proceeding with the solution of the problem at hand.

First we note that, as shown on page 200 of Ref. 12, there is a relation between the coefficients J, H, P, G , which may be written as

$$\frac{3}{2} J = (P^2 + GH) / P. \quad (3.9)$$

It also turns out that in all static applications of the droplet model the equilibrium distributions of the neutrons and protons are such that the local neutron skin thickness t is related to the local surface neutron excess δ_s by [Eq. (46), p. 198, Ref. 12]:

$$\frac{t}{\delta_s} = \frac{G}{P} r_0 \quad (3.10)$$

$$= \frac{3}{2} \frac{J}{Q} r_0, \quad (3.11)$$

where

$$Q \equiv \frac{3JP}{2G} = H / \left(1 - \frac{2}{3} \frac{P}{J}\right) \text{ in virtue of Eq. (3.9).} \quad (3.12)$$

The above combination of coefficients has special significance in the droplet model. This can be appreciated by inserting Eq. (3.11) in the surface-energy integral in Eq. (3.7) which then reduces to

$$\frac{1}{4\pi r_0^4} \int_{\text{surf}} Q t^2. \quad (3.13)$$

Thus Q has the significance of a stiffness coefficient against the formation of neutron skin t , when this skin is accompanied, at each point on the surface, by a local neutron excess δ_s related to t by Eq. (3.11). Note the distinction between this stiffness Q and the stiffness against the formation of a neutron skin at constant δ_s , which is given by H . The relation between t and δ_s , given by Eq. (3.11), is predicted to hold in the droplet model theory for the equilibrium density distributions

of semi-infinite or finite systems, with or without Coulomb energy, and for spherical or nonspherical shapes. We shall refer to it as the "droplet rule" and we shall see later the relevance of this static rule for the dynamics of the giant dipole oscillation.

In such an oscillation the amplitude of the neutron skin thickness vibrations at a point specified by θ is given by

$$\tau = -\alpha_1 A^{1/3} \cos\theta \quad (3.14)$$

and the amplitude of the neutron excess vibrations at point r, θ is given by

$$\delta = -2\alpha_2 \left(\frac{NZ}{A^2}\right) K j_1(kr) \cos\theta, \quad (3.15)$$

which reduces to

$$\delta_s = -\frac{1}{2} \alpha_2 a^2 \cos\theta \quad (3.16)$$

for a point of the surface (we again replaced NZ/A^2 by $1/4$).

The integrals in Eq. (3.7) can be performed after substituting Eqs. (3.14)–(3.16). The resulting expression in α_1 and α_2 can be compared with Eq. (3.2) in order to establish that the components of \underline{C} are

$$\begin{aligned} C_{11} &= \frac{2}{3} HR^4 / r_0^4 \approx \frac{2}{3} HA^4 / 3, \\ C_{12} = C_{21} &= \frac{1}{3} Pa^2 R^3 / r_0^3 \approx \frac{1}{3} PAa^2, \\ C_{22} &= \frac{1}{4} JA a^2 (a^2 - 2) - \frac{1}{6} Ga^4 R^2 / r_0^2 \\ &\approx \frac{1}{4} JA a^2 (a^2 - 2) - \frac{1}{6} GA^2 / 3 a^4. \end{aligned} \quad (3.17)$$

Note that C_{11} , which is the coefficient describing the restoring force in the GT mode, is proportional to the droplet model coefficient H rather than to J (the volume symmetry energy coefficient) as was assumed in Ref. 3. The coefficient H describes the resistance against the formation of a neutron skin. Another point to note is that the coefficient C_{22} , corresponding to the SJ mode, consists not only of the usual volume term proportional to J , but also of a surface term proportional to the droplet model coefficient G .

The off-diagonal terms C_{12} and C_{21} provide the potential energy coupling between GT and SJ modes because of the joint dependence of the surface energy on τ and δ_s . In addition the two modes are inertially coupled through the terms B_{12} and B_{21} in the inertia matrix.

IV. SOLUTIONS

Equation (3.1) has solutions only when the determinant of the coefficients vanishes,

$$\det(\omega^2 \underline{B} - \underline{C}) = 0, \quad (4.1)$$

which leads to the expression

$$\omega_{\pm} = \left\{ \frac{D \pm [D^2 - 4 \det(\underline{B}) \det(\underline{C})]^{1/2}}{2 \det(\underline{B})} \right\}^{1/2}, \quad (4.2)$$

where

$$D = B_{11}C_{22} - 2B_{12}C_{12} + B_{22}C_{11}. \quad (4.3)$$

The resulting quantized eigenenergies of the harmonic vibrations of the system are

$$E_{\pm} = \hbar\omega_{\pm}. \quad (4.4)$$

The energy E_{-} is the dipole vibration to be compared with the mean energy E_m of the GDR. The energy E_{+} corresponds to a higher-lying oscillation for which the GT and SJ modes are nearly out of phase and whose dipole moment nearly vanishes

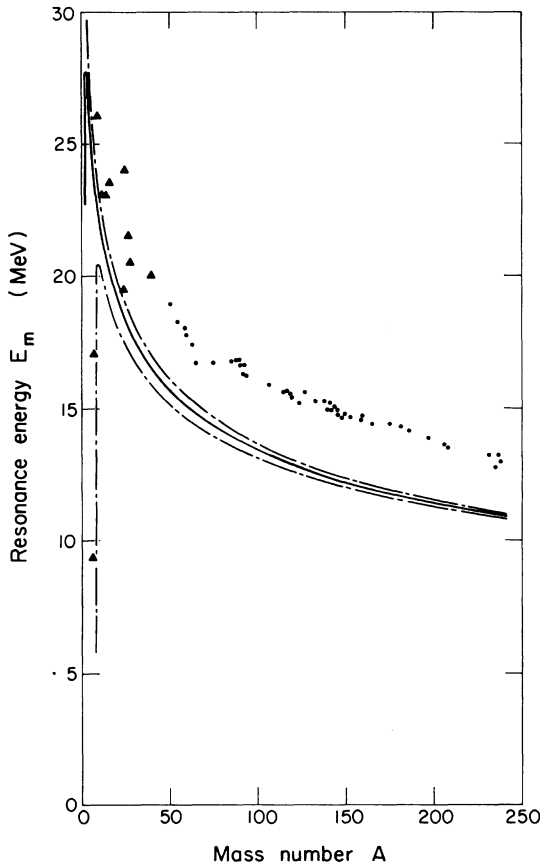


FIG. 2. The measured values of the mean energy E_m of the GDR are plotted against the mass number A . The dots are from the Lorentz curve fits of Ref. 2 [slightly improved values are now available (Ref. 16)] and the triangles are from Refs. 1 and 15. The solid curve corresponds to the predictions of Eq. (4.4) for a set of droplet model coefficients derived from a fit to nuclear masses [case (b) in Table I]. The upper and lower curves correspond to cases (a) and (c) in Table I. These were chosen to illustrate the effect of making substantial variations in the coefficients (while minimizing the impact on the fit to masses).

TABLE I. Different sets of droplet model coefficients (in MeV) corresponding to the curves shown in Fig. 2.

Curve	Q	J	H	P	G
(a) Upper	20	32.11	16.47	8.50	20.47
(b) Middle	17	36.8	14	9.74	31.63
(c) Lower	14	46.52	11.53	12.31	61.36

(see later).

The nature of the eigenvibrations as regards the relative amounts of the SJ and GT modes is given by the ratios $(\alpha_2/\alpha_1)_{\pm}$ associated with the ω_{\pm} solutions. They follow from the expression

$$(\omega_{\pm}^2 \underline{B} - \underline{C}) \cdot \underline{\alpha} = 0, \quad (4.5)$$

which leads to

$$\left(\frac{\alpha_2}{\alpha_1} \right)_{\pm} = - \frac{\omega_{\pm}^2 B_{11} - C_{11}}{\omega_{\pm}^2 B_{12} - C_{12}}. \quad (4.6)$$

Figure 2 shows a comparison of the calculated energy $\hbar\omega_{-}$ with experiment. The middle curve is for a set of nuclear parameters given by a recent droplet model fit to nuclear masses, fission barriers, and radii (Ref. 13), viz. $J = 36.8$ MeV, $Q = 17$ MeV, $r_0 = 1.18$ fm. An illustrative value of $H = 14$ MeV was assumed. The values of $P = 9.74$ MeV and $G = 31.63$ MeV then follow from Eqs. (3.9) and (3.12). [This is case (b) in Table I]. The upper and lower curves are for $Q = 20$ MeV and $Q = 14$ MeV, with J adjusted to 32.11 and 46.52 MeV, respectively. This adjustment tends to minimize the damage done to the fit to nuclear masses by the departure from the optimum values of J and Q . The ratio of $H:Q$ for all three curves was maintained at 14:17.

Even though Eqs. (4.1) and (4.5) are explicit solutions in the closed form of the coupled equations of motion, their dependence on the nuclear parameters J, Q, H, P, G is not transparent. Fortunately two excellent approximations to the exact solution are available, which display this dependence in a simple and illuminating manner.

A. Supersimple solution

This solution makes use of the fact that the determinant of the inertia matrix is nearly equal to zero. Thus if the quantity a were exactly 2 (instead of 2.08), making $\frac{1}{2}(a^2 - 2)$ exactly 1, the determinant of \underline{B} would vanish and it is readily verified that the resulting equations of motion would have the following simple solution for the dipole mode of oscillation:

$$\frac{1}{\omega_-^2} = \frac{m r_0^2}{8J} A^{2/3} + \frac{3m r_0^2}{8Q} A^{1/3}. \quad (4.7)$$

$$= \frac{m R_0^2}{8J} (1+u), \quad (4.8)$$

where u stands for $(3J/Q)A^{-1/3}$.

The associated ratio of the SJ to the GT mode is

$$(\alpha_2/\alpha_1)_- = (Q/3J)A^{1/3} = u^{-1}. \quad (4.9)$$

In this supersimple approximation the solution depends only on J and Q .

B. Droplet mode solution

We note that the relation for α_2/α_1 given by Eq. (4.9) is equivalent to the statement that, for the oscillation in question, the ratio of the local skin thickness t to the local neutron excess δ_s is given by

$$\frac{t}{\delta_s} = \frac{-r_0 \alpha_1 A^{1/3} \cos \theta}{-\frac{1}{2} \alpha_2 \cdot 4 \cdot \cos \theta} = \frac{3J}{2Q} r_0 \quad (4.10)$$

independently of position on the surface. We recognize this as the universal relation predicted by the static droplet model for the equilibrium ratio of the neutron skin thickness to the neutron excess at the surface.^{11,12} (The droplet rule—see above.)

Taking this as a hint we may construct an approximate solution of the coupled equations by imposing the restriction $t/\delta_s = (3J/2Q)r_0$, i.e.,

$$\frac{\alpha_2}{\alpha_1} = \frac{4}{a^2} u^{-1}, \quad (4.11)$$

but without making the approximation $a=2$. With the above restriction the problem is now an oscillation in one degree of freedom, with the single solution:

$$\omega^{-2} = \frac{m R_0^2}{8J} \left(1+u - \frac{1+\epsilon+3u}{1+\epsilon+u} \epsilon \right), \quad (4.12)$$

$$\alpha_2/\alpha_1 = (1-\epsilon)u^{-1}, \quad (4.13)$$

where ϵ is a small quantity, defined by

$$\begin{aligned} \epsilon &= 1 - (4/a^2) \\ &= 0.0768. \end{aligned} \quad (4.14)$$

This solution still depends only on J and Q .

In a typical case ($A=125$) the supersimple solution (4.8) gives an energy $\hbar\omega$ which is accurate to 0.42 MeV, or 3.2%. The droplet mode solution (4.12) gives $\hbar\omega$ accurate to 0.04 MeV, or 0.3%. The latter solution in particular may be used as an essentially exact expression for $\hbar\omega$, agreeing with the plot in Fig. 2 to within the width of the line in most cases of interest.

The values of α_2/α_1 predicted by the exact solu-

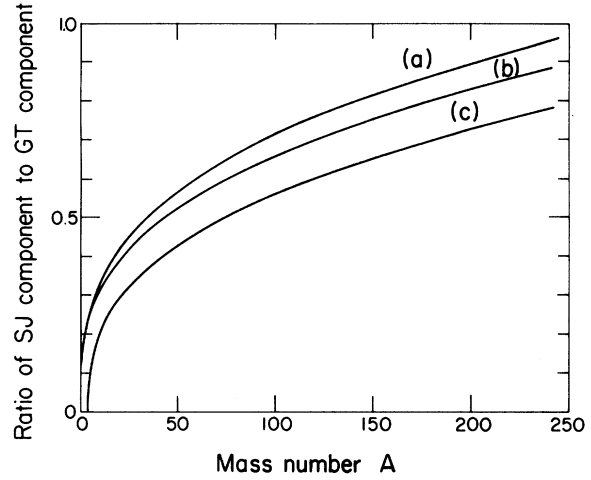


FIG. 3. The ratio (α_2/α_1) of the SJ component to GT component in the GDR is plotted against mass number A for three different cases of interest. Curve (a) corresponds to the supersimple solution, Eq. (4.9); curve (b) to the droplet mode, Eq. (4.13); and curve (c) to the exact solution given by Eq. (4.6). In all these cases the droplet model coefficients given in row (b) of Table I were used.

tion and the above two approximations are compared in Fig. 3. We see that the GT mode tends to dominate for light nuclei and that it contributes more than the SJ mode for all mass numbers in the Periodic Table. The amount of the SJ mode increases with A and almost reaches parity for the heaviest nuclei.

In order to illustrate the nature of the actual density oscillations we show in Fig. 4 the appearance of the density distributions at the instant of maximum displacement (the classical turning point of the quantized oscillation) for ^{208}Pb . The centers of the neutron and proton spheres are seen dis-

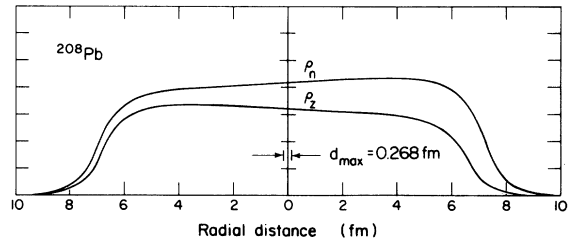


FIG. 4. The neutron and proton density profiles along the GDR symmetry axis are plotted against distance from the center of mass for the case of ^{208}Pb . The centers of the effective sharp spherical boundaries of the two density distributions (GT mode) are shown displaced from each by the maximum distance that is expected to occur during the vibration (0.268 fm). The corresponding compressional pileup (SJ mode) of neutrons on one side and protons on the other is also indicated.

placed by about 0.27 fm, and there is a considerable difference in the values of the local neutron excess at the left- and right-hand tips of the nucleus.

V. COMPARISON WITH EXPERIMENT

The most noticeable feature of Fig. 2 is the discrepancy of about 15% between the absolute values of the calculated curves and experiment. As pointed out above the calculations depend for all intents and purposes only on J and Q , and no reasonable changes in these coefficients, consistent with fits to nuclear masses, can bring the curves into agreement with experiment.

Using Eqs. (4.8) or (4.12) we may readily determine the values of J and Q that would be demanded by the GDR data. Thus from Eq. (4.8) it follows that if the quantity $8/(mR_0^2\omega^2)$ is plotted against $A^{-1/3}$ a straight line should result, with J^{-1} as the intercept on the ordinate axis and $3Q^{-1}$ as the slope. If the more accurate Eq. (4.12) is used, such a plot should also conform closely to a straight line, but with the intercept equal to about $0.88J^{-1}$ and slope about $0.97(3Q^{-1})$. (See Appendix C.) Figure 5 shows this type of plot. We see that the data for $A \geq 50$ define reasonably

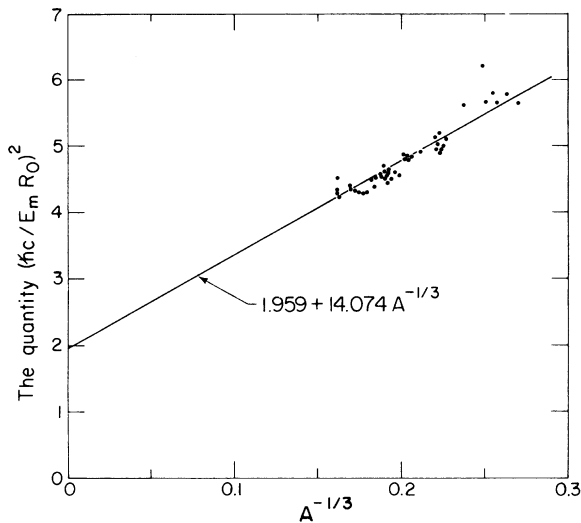


FIG. 5. The quantity $(\hbar c/E_m R_0)^2$ is plotted against $A^{-1/3}$ for nuclei with $A > 50$. These points are expected to lie approximately on a straight line given by $m^*c^2/8 [0.8772 J^{-1} + 0.9707 (3Q^{-1})A^{-1/3}]$ see Appendix C. For the values of the droplet model coefficients $J=36.8$ MeV and $Q=17$ MeV determined from nuclear masses (Ref. 13) [case (b) in Table I] we find that agreement can only be obtained by assuming an effective mass m^* less than m . A value of $m^*=0.69m$ gives the best agreement with the experimental data but we have chosen to round this off to $0.7m$ for simplicity. The straight line in the figure corresponds to this choice for m^* .

well a linear trend. (For $A \leq 50$ there is more scatter in the experimental points.) This confirms roughly the correctness of the functional form of the A dependence predicted by the model of coupled GT and SJ oscillations, but the values of the coefficients J and Q associated with the intercept and slope of the line in Fig. 5 are $(0.7)^{-1}$ times bigger than the values $J=36.8$ MeV, $Q=17$ MeV determined from the fit to masses. This apparent discrepancy could be an indication that the effective inertia involved in the oscillations of the neutrons against the protons was somewhat smaller than the inertia of the bodily motions of the neutron masses against the proton masses. The reason might be that part of the time the neutrons and protons exchange character (in virtue of the exchange component of the nucleon-nucleon force) without actually undergoing the associated displacements in space.

(The exchange component of the interaction between nucleons is also known to contribute to the enhancement of the total dipole absorption cross section over its sum rule value.¹⁷⁻¹⁹) If we represent this effect by introducing effective inertial mass densities for the neutron and proton fluids by $\rho_{n,z}^* = (m^*/m)\rho_{n,z}$ (this m^* is not necessarily the quantity governing the density of single-particle levels at the Fermi surface) we may still use all the formulas derived so far but with m replaced everywhere by m^* .

Figure 6 shows that once an effective mass m^* equal to $0.7m$ is assumed there is perfect agreement with the droplet model prediction for the trend of $\hbar\omega$, based on the standard coefficients $J=36.8$ MeV, $Q=17$ MeV.

By contrast it is clear, especially from Fig. 5, that the trend with A in the observed energies is inconsistent with either a pure Goldhaber-Teller or a pure Steinwedel-Jensen model. In the former case the data points in Fig. 5 should lie along a line through the origin; in the latter they should form a horizontal line. The same fact had been brought out by the extensive analysis in Ref. 2, which demonstrated empirically a transition from a proportionality of $\hbar\omega$ to $A^{-1/6}$ for small A to a proportionality to $A^{-1/3}$ for large A . The essential agreement with theory in this respect may be exhibited by rewriting Eq. (4.8) in the form

$$\omega^{-1} = \left(\frac{m r_0^2}{8J} \right)^{1/2} A^{1/3} [1 + (A_0/A)^{1/3}]^{1/2}, \quad (5.1)$$

where

$$A_0 \equiv (3J/Q)^3 \approx 274. \quad (5.2)$$

[A similar relation follows approximately from Eq. (4.12).] Thus, as noted in Ref. 2, the mass number characterizing the transition region where

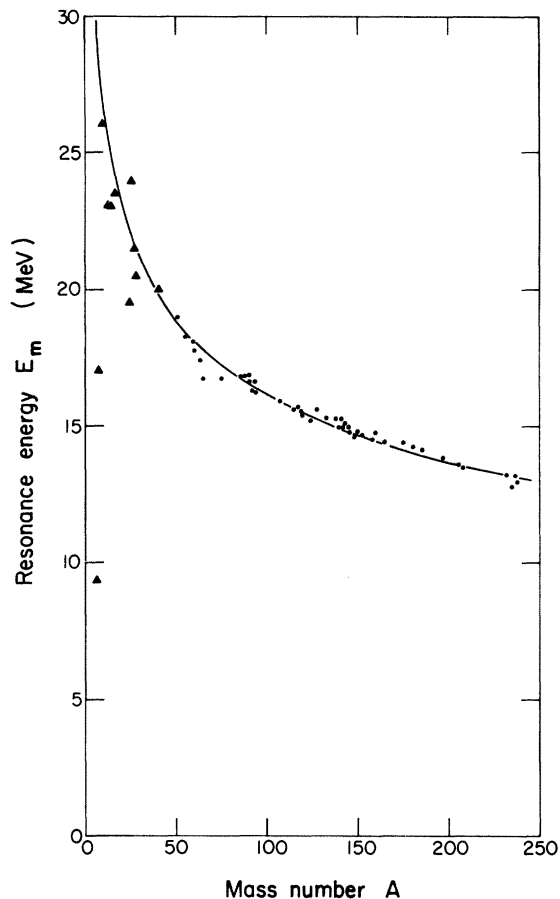


FIG. 6. The measured values of the resonance energy E_m are plotted against mass number A , as in Fig. 2. The curve passing through the points corresponds to the predictions of Eq. (4.12) with $J=36.8$ MeV, $Q=17$ MeV, and an effective mass $m^*=0.7m$.

neither the GT nor the SJ behavior is appropriate lies near the end of the Periodic Table. We also realize now that one-third of the cube root of this characteristic mass number is a measure of the ratio of the symmetry energy J to the effective neutron skin stiffness Q . The GDR energies thus provide an independent estimate of this ratio, which agrees with the value determined from nuclear masses ($J:Q=36.8:17$).

We may also note that if the GDR frequency ω is calculated under the restriction of a pure SJ mode the result has to exceed the value of ω obtained without this restriction. This may be the reason why in past analyses of the GDR, restricted artificially to a pure SJ mode, the need for an effective mass less than m was not apparent,²⁰ the inaccuracy of the restricted solution accidentally tending to produce agreement with the experimental resonance energies.

VI. DISCUSSION

The situation emerging from the above analysis is something like this: In 1948 Goldhaber and Teller pointed the way towards an interpretation of the giant dipole resonance in terms of a simple oscillation of rigid neutron and proton spheres. This was largely replaced in 1950 by the more sophisticated Steinwedel-Jensen model of an acoustical resonance. Due to the accumulation of excellent experimental data, especially by the Livermore and Saclay groups, it eventually became clear that neither the GT nor the SJ idealization was quantitatively satisfactory. The theory presented here, according to which the oscillating system is allowed to decide for itself the relative amounts of the GT and SJ modes, leads indeed to a situation where neither mode is expected to be dominant—and certainly not the SJ mode, which would not dominate until $A \gg 274$. (See Ref. 21 for a microscopic treatment leading to similar conclusions.) On the contrary, the mixture appears to be close to a special combination, the droplet mode which, for any value of A , is just such as to make the local neutron excess at any point on the surface and at any instant follow the local neutron skin thickness according to the droplet rule. The result is that even for lighter nuclei, with $A \ll 274$, when the A dependence of the resonance energy tends towards the Goldhaber-Teller $A^{-1/6}$ law, the actual value of the frequency is predicted to be governed by the effective neutron skin stiffness Q and *not* by the stiffness H , which would be appropriate for a pure GT mode [see Eq. (4.8)]. Thus *nowhere* in the Periodic Table is one justified in relying on an idealization of a pure GT or a pure SJ model.

What is the physical significance of the choice by the oscillating system of the droplet mode? Mathematically this is the result of the near vanishing of the determinant of the inertia matrix B . As is readily verified the kinematic meaning of this near vanishing is the similarity of the flow patterns in the GT and SJ modes of oscillation. In general, if two modes of motion have essentially the same flow patterns (and are regarded as separate modes only because the potential energy is different for them) then the off-diagonal (cross) term in the kinetic energy, involving the product of the time derivatives of the two modes, is no different (apart from normalization) from the diagonal terms which involve the squares of the time derivatives of each mode separately. The inertia matrix can then be brought to the form

$$\begin{pmatrix} 1 & 1 \\ 1 & 1 \end{pmatrix}$$

for which the determinant is clearly zero. It is apparently because the GT and SJ flow patterns are (somewhat surprisingly) quite similar, at least in an integral sense, that it is left largely for the potential energy to decide on the optimum mixture of the two modes, with the result that the mixture conforms closely to the static droplet rule.

One aspect of the similarity of the GT and SJ flow patterns is that they are by and large not too far from parallelism, i.e., that also in the SJ mode the oscillation is largely a to-and-fro motion of the nucleons parallel to the direction of the electric field. The recognition of this feature may be relevant for the microscopic interpretations of the GDR. Insofar as the gross motions induced by the electric field are parallel displacements, one might expect the nodal structure of the individual particle wave functions not to change very much. Consequently, the inertia of the oscillations, as calculated microscopically for the quantized nucleons, might be expected to be much closer to the hydrodynamical value than if drastic rearrangements of the nodal structures were involved (Ref. 22). This feature would be even more in evidence for nuclear potentials (such as a harmonic oscillator well) for which the motion along the axis of the field is separable from the transverse directions. This should help to explain why the macroscopic hydrodynamic model appears to work reasonably well even as regards absolute values of the resonance frequency, in particular why there is no evidence at all in the data for inertias *exceeding* the hydrodynamical values. Altogether if one remembers that throughout the Periodic Table the major part of the oscillation is in the form of rigid displacements of the GT type, and that the remainder is also, in an integral sense, not too different from such a simple motion, one realizes that the proper role of a microscopic treatment of the GDR is to discuss the finer details of the motions, the overall behavior being quite well reproduced, for a good reason, in a macroscopic approach. After all, in describing center-of-mass displacements of a system, little is to be gained by starting with a microscopic many-body wave function of the A interacting particles constituting the system in question.

Concerning the subject of microscopic treatments of the GDR we should add one remark. Such treatments are more fundamental and contain, in principle, all the physics of a macroscopic treatment and, in addition, all the subtleties, refinements, and peculiarities associated with the retention of the particle degrees of freedom. However, if a microscopic treatment is to be relevant in its quantitative predictions it must, in practice,

contain the physical features that are associated with the two principal restoring forces of the GDR, namely the symmetry energy J and the effective neutron skin stiffness Q . This implies that the effective nuclear interaction used in a microscopic treatment must be chosen so that it could reproduce the experimental values of J and Q . Also the techniques employed in the solution (e.g., the parametrization of the potential well and the amount of configuration mixing allowed) should be adequate to describe accurately bodily displacements of the neutrons and protons. Only then can one usefully relate the difference between the results of microscopic and macroscopic treatments to the refinements associated with the retention of the particle degrees of freedom.

VII. ESTIMATE OF WIDTH

We shall present a tentative estimate of the width of the GDR based on the recently formulated one-body damping expression.²³⁻²⁶ The rate of energy dissipation \dot{E} is written as

$$\dot{E} = \rho \bar{v} \oint_{\text{surf}} \dot{n}^2 d\sigma, \quad (7.1)$$

where ρ is now the mass density and \bar{v} the average particle speed of a long mean-free-path gas in a container whose wall elements $d\sigma$ are moving with normal speeds \dot{n} with respect to the bulk of the gas (i.e., with respect to its center of mass). In our case there are two gases, the neutrons and the protons, and the average particle speed is $\frac{3}{4}$ of the Fermi velocity v_F . The container is the potential well felt by the neutrons or protons. We shall assume that the surface of this well remains stationary because it is determined principally by the *total* density, whose boundary does not move very much as the neutrons and protons oscillate against each other. The relevant relative velocity component \dot{n}_z for the protons, say, is then just minus the velocity of the center of mass of the protons, projected onto the normal of a surface element $d\sigma$. Since the dipole moments D_1, D_2 given by Eqs. (2.4) and (2.11) are simply related to the center-of-mass locations of the protons and neutrons we readily find

$$\dot{n}_z = -\frac{N}{A} (\dot{\alpha}_1 + \dot{\alpha}_2) R \cos \theta, \quad (7.2)$$

$$\dot{n}_n = \frac{Z}{A} (\dot{\alpha}_1 + \dot{\alpha}_2) R \cos \theta.$$

The rate of energy dissipation follows as:

$$\dot{E} = D \dot{\alpha}^2, \quad (7.3)$$

where

$$D = mAR\bar{v}(NZ/A^2) \quad (7.4)$$

and

$$\alpha = \alpha_1 + \alpha_2. \quad (7.5)$$

In the supersimple approximation the kinetic energy may be written as

$$T = \frac{1}{2} B \dot{\alpha}^2, \quad (7.6)$$

where

$$B = mAR^2(NZ/A^2). \quad (7.7)$$

In the same approximation the potential energy (not needed for an estimate of the width) is

$$V = \frac{1}{2} C \alpha^2, \quad (7.8)$$

where

$$C \approx \frac{2}{3} QA^{4/3}u/(1+u). \quad (7.9)$$

The equation of motion for α is then

$$B\ddot{\alpha} + D\dot{\alpha} + C\alpha = 0. \quad (7.10)$$

The predicted width of the resonance is given by the delightfully simple expression

$$\Gamma = \hbar \frac{D}{B} = \hbar \left(\frac{\bar{v}}{R} \right). \quad (7.11)$$

The widths given by Eq. (7.11) are predicted to vary as $A^{-1/3}$. The calculation is compared with experiment in Fig. 7 and there is no order-of-magnitude disagreement between the experimental

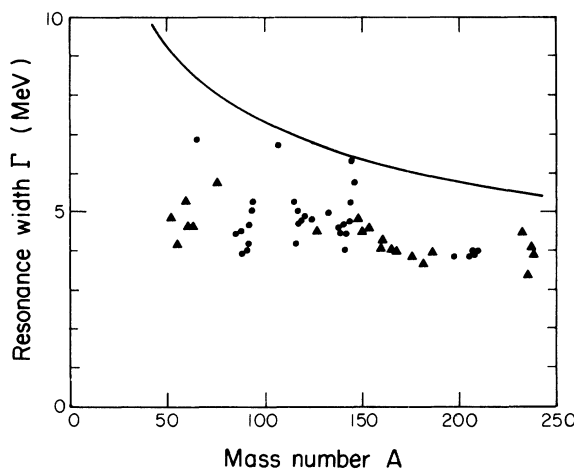


FIG. 7. The measured width Γ of the GDR (obtained from the Lorentz curve fits of Ref. 2) is plotted against the mass number A . The dots correspond to single Lorentz curve fits to (presumably) spherical nuclei, while the triangles correspond to mean values for deformed nuclei calculated from the expression $\Gamma = (\Gamma_1 \Gamma_2)^{2/3}$, where Γ_1 and Γ_2 are the measured widths of the two components of the resonance. The solid curve corresponds to the predictions of Eq. (6.11) which is based on the concept of one-body damping (Ref. 23).

values and the theory. Note that the theory has no adjustable parameters since the one-body dissipation formula has no adjustable viscosity coefficient. (This may be contrasted to ordinary hydrodynamic treatments of nuclear dynamics, or with theories that postulate frictional forces between interpenetrating density distributions in relative motion.²⁷⁻²⁹ Also the effective mass m^* which, to a certain extent, was a parameter in the fit to the resonance energies, cancels out in the expression for the width. It will be interesting to continue testing the macroscopic nuclear dynamics predicted by the one-body dissipation theory in a variety of situations, such as the GDR, where microscopic features appear to play a secondary role.

VIII. SUMMARY

The principal results of this study are as follows:

- (1) The application of the droplet model to the GDR leads to a simple algebraic theory.
- (2) The relative amounts of the Goldhaber-Teller and Steinwedel-Jensen modes of oscillation are found to be such that in general neither dominates. The mixture conforms closely to the static droplet model rule.
- (3) This is the result of the (unexpected) finding that the flow pattern for the SJ mode of oscillation is very similar, in an integral sense, to the GT motion (a to-and-fro oscillation parallel to the electric field).
- (4) A comparison of the resonance energies with experiment shows a firm discrepancy of 15% in absolute magnitudes, which may be evidence that the effective inertial mass in the dipole vibration is less than the inertial mass associated with bodily displacements of the neutrons and protons.
- (5) With an effective mass $m^* = 0.7m$ inserted in the theory the agreement with the experimental A dependence of the GDR energy is excellent.
- (6) The observed transition from a proportionality of $\hbar\omega$ to $A^{-1/6}$ to a proportionality to $A^{-1/3}$ is correctly reproduced, and the GDR data may be used to give an independent estimate of the ratio of the effective neutron skin stiffness coefficient Q to the symmetry energy coefficient J . The result is in agreement with the value deduced from a droplet model fit to masses, ($Q : J = 17 : 36.8$).
- (7) An estimate of the width of the GDR, based on the one-body dissipation formula of Refs. 23-26, is not in qualitative disagreement with the data.

The authors wish to acknowledge a number of important discussions with B. L. Berman, and useful comments from G. F. Bertsch, A. Z. Mekjian, and K. Takahashi.

APPENDIX A. DEPENDENCE OF SOLUTIONS ON H

The exact solution of the coupled equations depends on the four coefficients J, H, P, G , but since there is one relation between them [Eq. (3.9)] there are only three independent parameters, which may be taken as J, Q , and H . As discussed above, the main dependence of the dipole frequency is on J and Q . The dependence on H is relative to the finiteness of ϵ , since if ϵ were zero the resulting solution for the dipole frequency, Eq. (4.8), would be strictly independent of H . However, even in the limit of $\epsilon \rightarrow 0$, the nature of the solutions as regards their *stability*, is directly related to H . This may be seen by examining the determinant of the stiffness matrix C . We find that in the limit $\epsilon = 0$ this determinant is proportional to $HA^{1/3} - 2P$ which, in virtue of Eq. (3.12), may be written as

$$\det \underline{C} \propto H[A^{1/3} - 3J(1/H - 1/Q)]. \quad (\text{A1})$$

Thus, for a given (positive) value of H , $\det \underline{C}$ is positive (and the system is stable) if A is large enough. The determinant changes sign, however, and the system acquires one degree of instability, if A decreases below A_{crit} , where

$$A_{\text{crit}}^{1/3} = 3J \left(\frac{1}{H} - \frac{1}{Q} \right). \quad (\text{A2})$$

Thus if $H > Q$ all (positive) values of A correspond to stable systems, but if H were less than Q then light nuclei with $A < A_{\text{crit}}$ would be unstable and any solutions of the associated equations of motion would involve at least one unstable mode.

In the case $J = 46.52$ MeV, $Q = 14$ MeV, $H = 11.53$ MeV, used as an illustration for the lower curve in Fig. 2, Eq. (A2) gives $A_{\text{crit}} = 9.74$. This is an estimate of the point where the lower curve in Fig. 2 abruptly dives down to zero, the estimate being based on the approximation where ϵ is as-

$$\omega_{\pm}^2 = \frac{2J}{mR_0^2} \frac{1}{\epsilon(1-\epsilon)} \frac{1}{u} \{ (1+u) + \epsilon u - \epsilon^2 \pm [(1+u)^2 + (2u^2 - 6u)\epsilon + (u^2 - 2u - 2)\epsilon^2 + 6u\epsilon^3 + \epsilon^3]^{1/2} \}, \quad (\text{B1})$$

where $u = (3J/Q)A^{-1/3}$ as before. For values of ϵ sufficiently small so that the square root may be expanded this reduces to

$$\omega_{+}^{-2} = \frac{mR_0^2}{4J} \frac{u}{1+u} \epsilon + \text{higher powers of } \epsilon, \quad (\text{B2})$$

$$\omega_{-}^{-2} = \frac{mR_0^2}{8J} (1+u) + \text{higher powers of } \epsilon. \quad (\text{B3})$$

The formula for ω_{-}^2 is the same to this order in ϵ as Eq. (4.8), and the ratio of ω_{+} to ω_{-} is

summed to vanish. It may be shown that in this approximation the dive to zero is exactly vertical, the smooth increase of ω_{-} as A decreases towards A_{crit} being reversed, without warning, in a sharp cusp at A_{crit} . This upward-pointing cusp is in fact the bottom part of a pair of intersecting curves, one of which is the smoothly rising curve continued into the region below A_{crit} , and the other a vertical line coming down from infinity. The effect of a finite ϵ is to break this level crossing (a pathological type of level crossing, where one "level" is a *vertical* line). This leads to two somewhat rounded cusps, the lower one corresponding to the solution ω_{-} illustrated in Fig. 2. The upper cusp corresponds to ω_{+} , a higher-frequency mode whose properties will be sketched out in the Appendix B.

APPENDIX B. "ANTIDIPOLE" RESONANCE

The frequency ω_{+} in the previous section, when plotted against A , has the appearance of a slightly rounded downward-pointing cusp. The right-hand part of the cusp rises abruptly to very high values (tending to infinity as ϵ tends to zero). Its left-hand part rapidly acquires the characteristics of the monotonic increase typical of the main part of the curves in Fig. 2. This part is associated with an oscillation of a system that has lost stability and is therefore of little physical interest. The right-hand part is a higher-frequency mode with practically zero dipole moment, where the GT and SJ modes are out of phase. It is, in principle, an interesting mode of oscillation. Its properties may be studied by solving Eq. (4.2) and (4.6) using the positive sign of the square root. A particularly simple way to illustrate the general nature of the solution is to consider the case when $H = Q$ (and therefore $P = G = 0$). The two frequencies are then readily found to be given by

$$\frac{\omega_{+}}{\omega_{-}} = \frac{1+u}{(2u\epsilon)^{1/2}}. \quad (\text{B4})$$

For a value of A equal to 125, when $u = 1.299$, this would give $\omega_{+}/\omega_{-} = 5.15$. Since $\hbar\omega_{-}$ is about 15 MeV, the higher-frequency mode would in this case be about 77 MeV. The actual predicted energy would vary with H (which, it will be recalled, was in the present example taken to be equal to Q) and it might also be more sensitive to the details of the theory than the dipole mode $\hbar\omega_{-}$. It would be of interest to pursue the question of the

existence, width, and possible ways of exciting this "antidipole" resonance which, formally at least, seems to follow from the well-established GDR by a reversal of the relative phases of the GT and SJ components.

APPENDIX C. GRAPHICAL DETERMINATION OF J AND Q

Even though Eq. (4.12) for ω^{-2} , unlike Eq. (4.8), is no longer linear in u (i.e., in $A^{-1/3}$) it is almost linear, since ϵ is small. By expanding the function of u appearing in Eq. (4.12) about u_0 , a point corresponding approximately to $A = 125$, the function may be linearized in the interval of A values of interest and the plot in Fig. 4 may still be used to extract the values of J and Q . Thus for u_0 we take $(3J/Q)(125)^{-1/3}$ which, with the nominal values of $J = 36.8$ MeV and $Q = 17$ MeV, leads to $u_0 = 1.2988$. The droplet mode expression for $1/\omega^2$ then becomes, to a good approximation,

$$\frac{1}{\omega^2} \approx \frac{mR_0^2}{8J} (0.8772 + 0.9707u) \quad (C1)$$

plus small terms of order $(u - 1.2988)^2\epsilon$ and higher. If an effective mass m^* is assumed we may write

$$\frac{8}{R_0^2\omega^2} \approx 0.8772(m^*/J) + 0.9707(3m^*/Q)A^{-1/3}. \quad (C2)$$

In Fig. 5 the quantity plotted against $A^{-1/3}$ is actually $c^2/8$ times the above, in order to make the ordinate dimensionless. The straight line through the points corresponds to a choice $J = 36.8$ MeV, $Q = 17$ MeV, $m^*/m = 0.7$.

We have also tried a slight modification of the plot in Fig. 5 which takes into account approximately the slight deviations of nuclear radii from the simple law $R = 1.18A^{1/3}$ fm. (The light nuclei have radii a few percent smaller than this.¹³) The net result on a plot of the type of Fig. 5 to move the upper points, corresponding to small values of A , a little to the right, without affecting appreciably any of the conclusions arrived at when this effect is neglected.

*Work supported in part by the U.S. Energy Research and Development Administration.

¹B. L. Berman, At. Data Nucl. Data Tables **15**, 319 (1975).

²B. L. Berman and S. C. Fultz, Rev. Mod. Phys. **47**, 713 (1975).

³M. Goldhaber and E. Teller, Phys. Rev. **74**, 1046 (1948).

⁴H. Steinwedel and J. H. Jensen, Z. Naturforsch. **52**, 413 (1950).

⁵M. Danos, Nucl. Phys. **5**, 23 (1958).

⁶J. M. Araújo, Nuovo Cimento **12**, 780 (1954).

⁷J. M. Eisenberg and W. Greiner, *Nuclear Models* (North-Holland, Amsterdam, 1970).

⁸A. Bohr and B. R. Mottelson, *Nuclear Structure* (Benjamin, New York, 1975), Vol. 2, Chap. 6.

⁹R. Bach and C. Werntz, Phys. Rev. **173**, 958 (1968).

¹⁰J. G. Brennan and C. Werntz, Phys. Rev. C **1**, 1679 (1970).

¹¹W. D. Myers and W. J. Swiatecki, Ann. Phys. (N.Y.) **55**, 395 (1969).

¹²W. D. Myers and W. J. Swiatecki, Ann. Phys. (N.Y.) **84**, 186 (1973).

¹³W. D. Myers, Lawrence Berkeley Laboratory Report No. LBL-3428, November, 1974 (unpublished).

¹⁴M. Tanaka and M. Yamada, in *Proceedings of Kawatabi Conference on New Giant Resonances, June 1975* (Research Report Suppl., Laboratory of Nuclear Science, Tohoku Univ. 1975), Vol. 8.

¹⁵J. Ahrens *et al.*, in *Proceedings of the International Conference on Photoneuclear Reactions and Applications, Asilomar, 1973*, edited by B. L. Berman (Lawrence Livermore Laboratory, Univ. of California, 1973) CONF-730301, pp. 23-41.

¹⁶B. L. Berman, B. F. Gibson, and J. S. O'Connell, Phys. Lett. (to be published), Table I.

¹⁷A. M. Lane and A. Z. Mekjian, Phys. Rev. C **8**, 1981 (1973).

¹⁸M. Danos, in *Proceedings of the International Conference on Photoneuclear Reactions and Applications, Asilomar, 1973* (see Ref. 15), p. 43-51.

¹⁹J. S. O'Connell, in *Proceedings of the International Conference on Photoneuclear Reactions and Applications, Asilomar, 1973* (see Ref. 15), pp. 71-93.

²⁰R. L. Bramblett, S. C. Fultz, and B. L. Berman, in *Proceedings of the International Conference on Photoneuclear Reactions and Applications, Asilomar, 1973* (see Ref. 15), pp. 13-22.

²¹G. Bertsch and K. Stricker, Phys. Rev. C **13**, 1312 (1976).

²²Kit-Keung Kan and J. J. Griffin, Phys. Rev. C **15**, 1126 (1977).

²³W. J. Swiatecki, Lawrence Berkeley Laboratory Report No. LBL-4296 (unpublished), presented at the International School Seminar on Reactions of Heavy Ions with Nuclei and Synthesis of New Elements, Dubna, USSR, 1975.

²⁴J. Randrup, Proceedings of the International Workshop on Gross Properties of Nuclei and Nuclear Excitations IV, Hirschegg, Austria, 1976 [Technische Hochschule Darmstadt Report No. AED-Conf-76-015-000, 1975 (unpublished)], pp. 69-76.

²⁵Y. Boneh, J. P. Blocki, and W. D. Myers, Phys. Lett. **63B**, 265 (1976).

²⁶J. P. Blocki *et al.*, Lawrence Berkeley Laboratory Report No. LBL-6100, January, 1977.

²⁷R. Wiczorek, R. W. Hasse, and G. Süßmann, in *Proceedings of the Third International Atomic Energy Agency Symposium on the Physics and Chemistry of Fission, Rochester, 1973* (IAEA, Vienna, 1974), IAEA-SM-174/02.

²⁸N. Auerbach and A. Yeverechyanu, Ann. Phys. (N.Y.) **95**, 35 (1975).

²⁹R. W. Hasse and P. Nervd, J. Phys. G **2**, L101-5 (1976).